Parameter design of a parallax barrier based on the color moiré patterns in autostereoscopic display

Lingsheng Kong,[1,2] Guang Jin,[1,*] Tiancong Wang,[1] Sheng Cai,[1] Xing Zhong,[1] and Kai Xu[1]

[1]Changchun Institute of Optics, Fine Mechanics and Physics, Chinese Academy of Sciences, Changchun, Jilin 130033, China

[2]Graduate School of the Chinese Academy of Sciences, Beijing 100039, China

*Corresponding author: jing@ciomp.ac.cn

Received 20 July 2011; revised 21 October 2011; accepted 22 October 2011; posted 27 October 2011 (Doc. ID 151411); published 18 November 2011

We propose a parameter design of the parallax barrier (PB) based on the color moiré patterns in autostereoscopic displays. First, the display device and the PB are approximated as two corresponding binary gratings. In order to obtain different corresponding predominant Fourier low-frequency terms, the superposition of the equivalent grating for the display device and the special radial grating is analyzed, referring to the indicial equation method and Fourier theory. Moreover, the two transition regions are considered as the regions where moiré patterns vary gently. Finally, the appropriate parameter of the PB can be obtained. The validity of the proposed design is verified in the experiment. © 2011 Optical Society of America

OCIS codes: 100.0100, 110.2650, 110.2990, 220.2740.

1. Introduction

As we all know, the superposition of periodic structures leads to moiré patterns. The moiré phenomenon is widely applied in many fields, such as strain analysis, topography, and moiré metrology, because of its sensitivity to the slightest displacements, variations, or distortions in the overlaid structures [1–7]. However, it is very necessary to avoid the moiré phenomenon in color printing [8,9]. At the same time, especially right now, many autostereoscopic display devices are assembled with several regular structures, such as LCD panels, parallax barriers (PBs), microlens arrays, and lenticular plates. Thus, the moiré phenomenon, which degrades the quality of an autostereoscopic image, is unavoidable in autostereoscopic displays [10]. Therefore, it is very important to reduce the chances of the appearance of the moiré phenomenon for practical purposes.

In previous works, two strategies have been mostly used to fight against undesired moiré patterns in autostereoscopic displays: avoiding moiré patterns (namely, preventing their generation) and minimizing moiré patterns (namely, reducing their appearance). For avoiding moiré patterns, one method is to change the layout of the color filter on the LCD [11,12]. However, the disadvantage of this method is the high cost in changing the layout of the color filter. Another method, which is proposed in [13], is to use defocusing and a diffuser. Besides avoiding moiré patterns, moiré minimization is also widely used in autostereoscopic displays. The most widely used method is to assemble the display device with slanted regular structures [14]. This method results in fine patterns, so that the moiré pattern becomes invisible in the autostereoscopic display. Recently, there were also some studies about moiré reduction by finding the optimal angle for superposing two grids for integral imaging [15–17].

PBs, lenticular sheets, and microlens arrays are the most widely used components in autostereoscopic displays. Particularly, integral imaging (II) using

0003-6935/11/34H153-06$15.00/0

microlens arrays is considered to be the most promising method [18–20]. The biggest advantage of this method is that it is able to provide continuous viewpoints and full parallax (both horizontal and vertical parallaxes). However, the resolution of the II autostereoscopic display degrades very fast. Therefore, one-dimensional (1D) II or multiview, which provides only horizontal parallaxes, is preferable in balancing the number of parallaxes and the resolution of the autostereoscopic display.

In this paper, moiré minimization is used to fight against moiré patterns. To obtain the appropriate parameters for the PB, several steps need to be carried out. First, the PB and LCD can be expressed as the corresponding binary gratings, as shown in Fig. 1. Thus, an autostereoscopic display using a PB can be approximated as the superposition of two corresponding binary gratings. To get the model of the PB with various parameters, a special radial grating is designed with a constant slit width. Apparently, this special radial grating can be considered an infinite number of PBs with different periods and grating vector directions [21]. We can find the predominant Fourier low-frequency terms in the case of different periods of the PB according to the superposition of the special radial grating and the equivalent binary grating of the LCD [7,22–24]. Finally, two transition regions are considered to be the proper regions without visible moiré patterns. Appropriate parameters of the PB can be confirmed by making moiré patterns almost unrecognizable to viewers' eyes.

2. Principle of the Mathematical Model

A. Equivalent Model of the LCD and the Parallax Barrier

Usually, an LCD panel display images via the combination of red (R), green (G), and blue (B) subpixels. As shown in Fig. 1(a), each color pixel is composed of three rectangular subpixels, and the width of the pixel (P_1) and subpixel (P) has the relationship of $P_1 = 3P$. According to [15], we can conclude that it is enough to consider only one color in the analysis of color moiré patterns. Thus, the strip-type color filter for any arbitrary one of the three colors can be represented as an erect binary grating, as in Fig. 1(b).

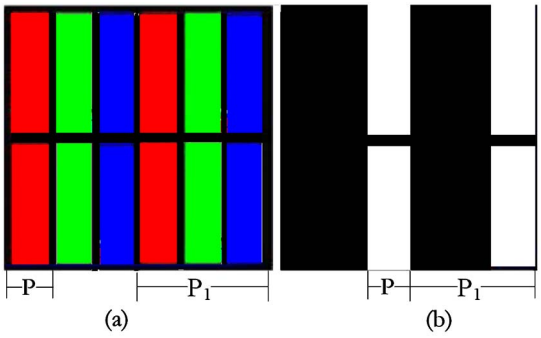

Fig. 1. (Color online) (a) Layout of LCD color filter; (b) the equivalent binary grating of an LCD.

The slit width and period of the erect binary grating coincide with P and P_1, respectively.

The PB provides the perspective views of a three-dimensional (3D) image by sampling the corresponding pixel among the pixels in its elemental image. The slit width P_s of the PB approximately equals the width of the subpixel, according to the multiview autostereoscopic displays theory [25]. According to [7], the angle of the PB influences only the angle θ and period P_m of a moiré pattern, not its amplitude. The amplitude and the profile of the moiré are affected by varying the opening ratio (here, namely, changes of period P_2 of the PB). Thus all the information of the moiré pattern is supposed to be analyzed with regards to P_2 and θ. Similar to an LCD, the binary grating with a constant slit width and varying slant angle and period is the equivalent model of the PB. Here the special radial grating, whose slit width is constant and equals the width of one subpixel, is considered a PB of progressively varying pitch and grating vector direction, as in Fig. 2 [21].

B. Simulation of Color Moiré Patterns

The color moiré pattern is simulated with regards to P_2 and θ. As shown in Fig. 1(b), the equivalent grating is two dimensional, so superposition of the LCD and PB can be considered superposition of three 1D gratings. In like manner, superposition of the LCD and the special radial grating is the superposition of two 1D gratings and a special radial grating. Because the amplitude and the profile of the moiré are affected only by varying the opening ratio, the longitudinal opening ratio of the black matrix is set to $1/3$ for simplicity. The superposition of the equivalent grating of the LCD and the special radial grating is shown in Fig. 3.

According to [15], a stable moiré-free state is achieved when the slant angle equals 26.61 deg. When the slant angle is less than 26.61 deg, the moiré patterns are consistent with the superposition of the 1D grating and the radial grating (see [5]). Thus, the black matrix can be neglected when the

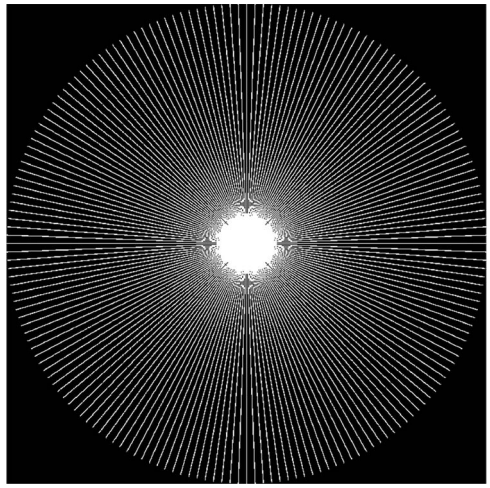

Fig. 2. Special radial grating.

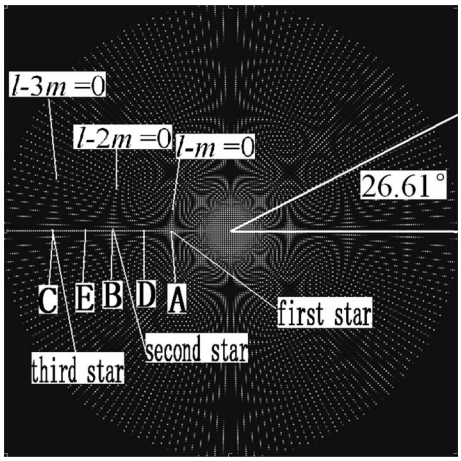

Fig. 3. Superposition of the special grating and the equivalent grating of LCD.

slant angle is less than 26.61 deg (namely, superposition of two 1D gratings is analyzed). Moreover, the slant angle of the PB in the 3D displays is usually small, so in this paper we define that the slant angle is less than 26.61 deg.

The PB located in front of the display device at a certain distance is rotated with the angle θ. The region $0 < \theta < 26.61°$ is the domain of the current problem. According to the assumptions in [15], three similar assumptions are given here. First, the distance between the display device and the PB is small enough in comparison to the observer distance. Second, the black matrix in the display device is negligible and the geometry of the RGB subpixels in the display device can be considered as being of the stripe type. Third, the test image is white images. In addition, the PB will weaken the brightness of the images, so the opening ratio of the PB is set larger than 0.1 (namely, P_2 is less than $10P$).

With these assumptions, the color moiré patterns can be analyzed by approximating 3D displays as two corresponding binary gratings. In addition, the relative translation between the LCD and the PB result in corresponding relative translation of moiré patterns, while it has no change about the period, angle, and intensity profile of the moiré patterns. Thus, we suppose that the equivalent grating of an LCD and a PB is symmetric. According to [7], the equivalent grating of an LCD can be expressed as

$$T_1(x,y) = \sum_{r=-\infty}^{r=\infty} a_r \cos(2\pi r x/P_1), \tag{1}$$

where a_r stands for the Fourier coefficient characterizing the amplitude and the phase of the nth harmonic. Similarly, the equivalent grating of the PB is represented as

$$T_2(x,y) = \sum_{s=-\infty}^{s=\infty} b_s \cos\left(\frac{2\pi s[x\cos\theta + y\sin\theta]}{P_2}\right), \tag{2}$$

where b_s designates the Fourier coefficients pertinent to the equivalent grating of the PB.

The combination of an LCD and a PB can be approximated as the superposition of T_1 and T_2. The result is given by the product of T_1 and T_2:

$$\begin{aligned} T(x,y) &= T_1(x,y)T_2(x,y) \\ &= \sum_{r=-\infty}^{r=\infty}\sum_{s=-\infty}^{s=\infty} a_r b_s \cos\left(\frac{2\pi r x}{P_1}\right) \\ &\quad \times \cos\left(\frac{2\pi s[x\cos\theta + y\sin\theta]}{P_2}\right). \end{aligned} \tag{3}$$

According to Eq. (3), we can conclude that there are infinite Fourier frequency terms of moiré patterns in the superposition of the LCD and the PB. However, different partial Fourier terms of moiré patterns still exist, and they are most visible to viewers' eyes when the period of the PB varies. Thus, it is necessary to find the relevant partial Fourier frequency terms, which are called predominant Fourier low-frequency terms. To find these predominant Fourier low-frequency terms, we analyze the superposition of the special radial grating and the equivalent grating of the LCD, as shown in Fig. 3. The indicial equation method is more appropriate for analyzing curved moiré patterns, so the equivalent grating of the LCD and the special radial grating can be expressed as the corresponding indicial equations. According to [5,21], the corresponding indicial equations are given as

$$y = lp, \tag{4}$$

where p is the width between lines and l is the order number of each line, and

$$\frac{x}{y} = \tan m\alpha, \tag{5}$$

where m is the order of the radial lines and α is the angle between each of the radial lines.

The unification of the indicial equation method and Fourier analysis is necessary for analysis of the moiré patterns in Fig. 3. According to [5,7,22], some necessary conclusions for the unification in the case of the superposition of two binary gratings are given first in Table 1, where R represents the partial terms of $T(x,y)$ and coincides with the corresponding families of curves referring to the indicial equation method.

Table 1. Unification of the Families of Curves and the Fourier Frequency Terms

Indexed Family of Curves	Corresponding Fourier Terms
$l - m = n$	$R_1 = T(x,y)$ $(r = -s)$
$l - 2m = n$	$R_2 = T(x,y)$ $(r = -2s)$
$l - 3m = n$	$R_3 = R(x,y)$ $(r = -3s)$

According to Eq. (4), the moiré patterns are shown in Fig. 4 in the case of the superposition of a line grating and a radial grating [5,21]. Figures 4(a)–4(c) show families of curves when m and n have the relationship of $l - m = n$, $l - 2m = n$, and $l - 3m = n$, respectively, where the cases of $n = 0$ are depicted by bold solid curves. In addition, the points labeled A, B, and C represent the equivalent positions where the equivalent periods are one, 2 times, and 3 times the line pitch. The families of curves $l - m = n$ and $l - 2m = n$ are shown in Fig. 4(d), and the curve $l - 1.5m = 0$ passes some points of intersection of $l - m = n$ and $l - 2m = n$. The curve $l - 2.5m = 0$ passes some points of intersection of $l - 2m = n$ and $l - 3m = n$. In like manner, the equivalent periods at points D and E are 1.5 and 2.5 times the line pitch, respectively. According to local similarities between Fig. 3 and the three families of curves $l - m = n$, $l - 2m = n$, and $l - 3m = n$, the different corresponding parts of the three families of curves are extracted. The right region of the curve $l - 1.5m = 0$ in Fig. 4(a) is eliminated, while the left region of the curve $l - 2.5m = 0$ in Fig. 4(c) is eliminated. For the region between the curves $l - 1.5m = 0$ and $l - 2.5m = 0$, the corresponding part of the indexed family of curves $l - 2m = n$ [Fig. 4(b)] is reserved. At last, the entire reserved region for the three families of curves $l - m = n$, $l - 2m = n$, and $l - 3m = n$ is shown in Fig. 4(f).

Similarities between the patterns can be observed by comparing the profiles of Figs. 3 and 4(f). These similarities indicate that the indexed family of curves $l - m = n$ are the predominant indexed family in the region around the first star pattern, while the indexed families of curves $l - 2m = n$ and $l - 3m = n$ are the predominant the indexed families in regions around the second and third star patterns, respectively. In addition, transition regions, namely, regions between two neighbored star patterns, have two predominant indexed families of curves. Concretely speaking, the indexed families of curves $l - m = n$ and $l - 2m = n$ exist in the transition region, which corresponds to the region around the curve $l - 1.5m = 0$. Likewise, the indexed families of curves $l - m = n$ and $l - 2m = n$ have the same strength in the transition region, which corresponds to the region around the curve $l - 2.5m = 0$.

As shown in Fig. 3, the moiré patterns in the transition regions change more gently, while the moiré patterns in other regions change strongly. Besides, there exists not only one predominant indexed family in the transition regions. We can conclude that moiré patterns are more invisible when the parameters of the PB fall into the transition region. There are two transition regions, which are around the curves $l - 1.5m = 0$ and $l - 2.5m = 0$. Obviously, there exist slight errors when the special radial gratings are considered as an infinite number of PBs with different periods and grating vector directions, so the corresponding exact value should be calculated according to Eqs. (1)–(3). For simplicity, the new

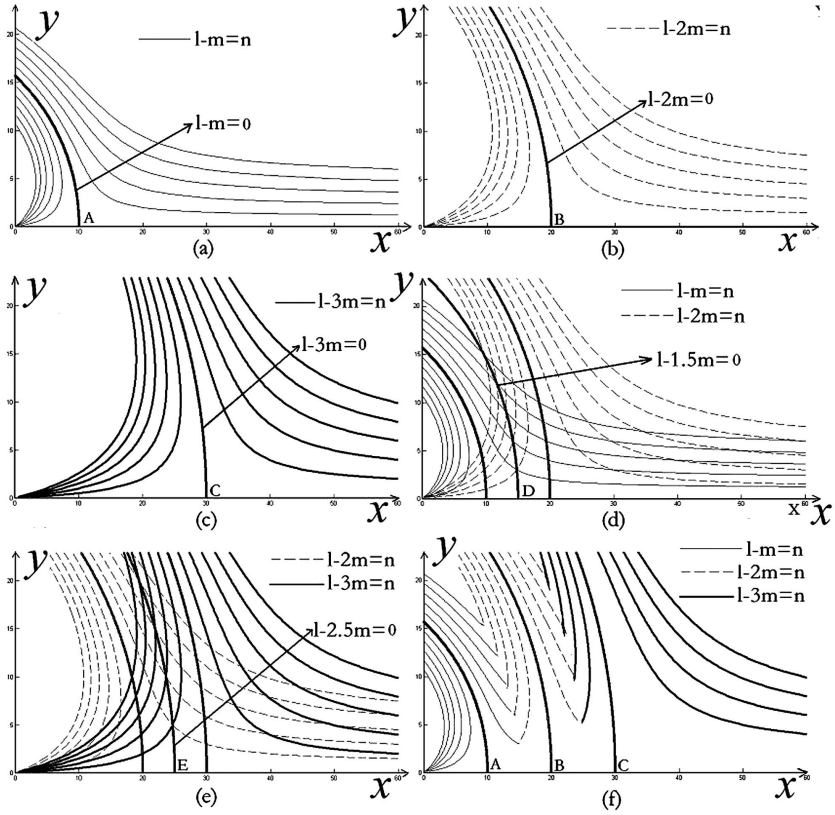

Fig. 4. (a) Indexed family of $l - m = n$; (b) the indexed family of $l - 2m = n$; (c) the indexed family of $l - 3m = n$; (d) the indexed family of $l - m = n$ and $l - 2m = n$; (e) the indexed family of $l - 2m = n$ and $l - 3m = n$; (f) the indexed family of $l - m = n$, $l - 2m = n$, and $l - 3m = n$.

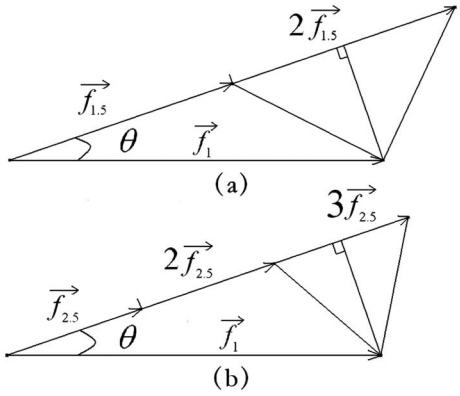

Fig. 5. Vectorial difference in the two transition regions.

corresponding vectors in the transition region are calculated by the vectorial difference of the frequency vectors of the original impulses [7]. Here we define that the periods of two corresponding predominant moiré patterns are equal in the transition regions. The vectorial differences in the transition region are shown in Fig. 5. It corresponds to the region around the curve $l - 1.5m = 0$ in Fig. 5(a). We can obtain

$$|\vec{f}_1 - \vec{f}_{1.5}| = |\vec{f}_1 - 2\vec{f}_{1.5}|, \tag{6}$$

where $\vec{f}_1$ is the fundamental frequency of the equivalent grating of the LCD and $\vec{f}_{1.5}$ is the fundamental frequency of the PB when moiré patterns correspond to the region around the curve $l - 1.5m = 0$. According to Fig. 5(a) and Eq. (1), we obtain

$$|\vec{f}_{1.5}| = \left|\frac{\vec{f}_1 * \cos(\theta)}{1.5}\right|. \tag{7}$$

Table 2. Predominant Fourier Low-Frequency Terms in the Transition Regions

P_2	Predominant Fourier Low-Frequency Terms
$4.5P/\cos(\theta)$	R_1, R_2
$7.5P/\cos(\theta)$	R_2, R_3

Table 3. Parameters of the Autostereoscopic Display Based on a PB

LCD	Size (inch)	19
	Resolution (pixel)	1280×1024
	P_1 (mm)	0.294×0.294
Parallax Barrier	P_s (mm)	0.095
	P_2 (mm)	0.756
	θ (°)	14.93
Autostereoscopic Display	Distance between LCD and PB (mm)	1.1
	View zone width (mm)	44
	View numbers	8
	View distance (mm)	500

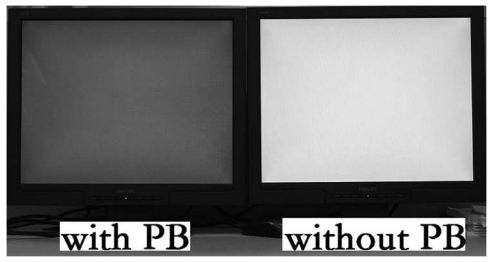

Fig. 6. Comparison of LCD image with and without the PB when the LCD image is white.

Thus,

$$P_2 = \frac{1.5P_1}{\cos(\theta)} = \frac{4.5P}{\cos(\theta)}. \tag{8}$$

In like manner, according to Fig. 5(b) and Eq. (1), we can obtain

$$P_2 = \frac{2.5P_1}{\cos(\theta)} = \frac{7.5P}{\cos(\theta)}. \tag{9}$$

From the discussion mentioned above, the predominant Fourier low-frequency terms in the different cases are summarized in Table 2, together with some inferences.

3. Experimental Results and Discussion

To obtain more view numbers, we choose the region around the curve $l - 2.5m = 0$. Generally speaking, there exists the similar viewing condition between color printing and autostereoscopic displays, so moiré patterns, which are larger than 1 mm, are considered to be visible in the autostereoscopic displays according to [7].

According to the discussion mentioned above, the optimal value of P_2 equals 0.761 mm, while P_1 equals 0.294 mm and θ equals 14.93 deg. However, the value of P_2 should be less than $8P\cos(\theta)$, referring to the multiview autostereoscopic displays theory, while the optimal value of P_2 is more than $8P\cos(\theta)$ [25]. Thus, taking into consideration the discussion mentioned above and multiview autostereoscopic displays theory simultaneously, a value of P_2 that is around 0.761 mm is selected. The parameters of the autostereoscopic display device are obtained and are listed in Table 3.

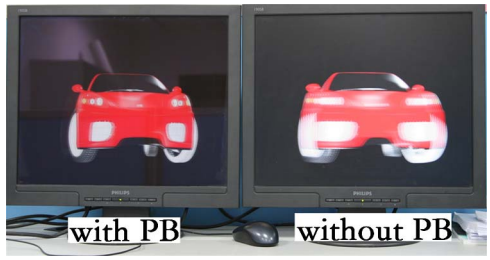

Fig. 7. (Color online) Autostereoscopic image comparison of an LCD with and without a PB.

The predominant Fourier low-frequency terms are R_2 and R_3 when $P_2 = 0.756\,\text{mm}$. According to the Fourier theory [7], the period of the moiré patterns, which corresponds to R_2 and R_3, are 0.89 and 0.93 mm respectively. The comparison of the LCD with and without the PB is shown in Fig. 6. A white image with weaker brightness is shown in Fig. 6. No visible moiré patterns are observed on these images, suggesting the images are in good quality.

The autostereoscopic images displayed in the LCD with and without the PB are exhibited in Fig. 7. A good image with validity of the PB parameter verified is shown in the left image of Fig. 7, while the right image is the ghost image because there is no PB. The comparison of these two images indicates that the designed PB is valid.

4. Summary

We propose a parameter design of the PB based on analyzing the color moiré pattern in an autostereoscopic display using the PB. Using this method, different significant moiré patterns (namely, predominant Fourier low-frequency terms) can be confirmed from the superposition of the equivalent grating of the LCD and the special radial grating. This proposed modeling method enables us to analyze the moiré pattern quantitatively in detail. $P_2 = 7.5P/\cos(\theta)$ is considered the best choice for the autostereoscopic display, and the appropriate slant angle can be calculated by using Fourier theory. The experimental results also show that a good autostereoscopic image can be obtained using our modeling method, whereas the designed PB is considered to be valid and available.

Furthermore, the color moiré pattern analysis is also suitable for an autostereoscopic display that uses a lenticular plate, which also provides only horizontal parallaxes.

References

1. K. Patorski, *Handbook of the Moiré Fringe Technique* (Elsevier, 1993), pp. 186–216.
2. O. Kafri and I. Glatt, *The Physics of Moiré Metrology* (Wiley, 1989), pp. 19–38, 75–87.
3. A. T. Shepherd, "25 years of moiré fringe measurement," Precis. Eng. **1**, 61–69 (1979).
4. H. Takasaki, "Moiré topography," Appl. Opt. **9**, 1467–1472 (1970).
5. A. J. Durelli and V. J. Parks, *Moiré Analysis of Strain* (Prentice-Hall,1970), pp. 64–78.
6. J. C. Wyant, *Moiré and Fringe Projection Techniques* (Wiley, 1992), pp. 653–681.
7. I. Amidror, *The Theory of the Moiré Phenomenon* (Springer, 2009), pp. 1, 9–21, 23–30, and 62.
8. J. P. Allebach, "Random nucleated halftone screen," Photogr. Sci. Eng. **22**, 89–91 (1978).
9. D. Blattner, C. Chaves, G. Fleishman, and S. Roth, *Real World Scanning and Halftones*, 3rd ed. (Peachpit, 2004), pp. 291–297.
10. K. Mashitani, G. Hamagishi, M. Sakata, A. Yamashita, E. Nakayama, and M. Inoue, "New autostereoscopic (no-glasses) LCD image splitter displays," in *3 Dimensional Image Conference '96* (Operating Committee of 3 Dimensional Image Conference, 1996), pp. 90–95.
11. K. Taira, R. Fukushima, T. Saishu, H. Kobayashi, and Y. Hirayama, "Autostereoscopic liquid crystal display using mosaic color pixel arrangement," Proc. SPIE **5664**, 349–359 (2005).
12. T. Koike, M. Oikawa, and K. Utsugi, "Moiré reduction for integral photography," in *International Display Workshops* (Society for Information Display, 2007), pp. 1917–1918.
13. M. Okui, M. Kobayashi, J. Arai, and F. Okano, "Moiré fringe reduction by optical filters in integral three-dimensional imaging on a color flat-panel display," Appl. Opt. **44**, 4475–4483 (2005).
14. L. Lipton and M. Feldman, "A new autostereoscopic display technology: the SynthaGram," Proc. SPIE **4660**, 229–235 (2002).
15. Y. Kim, G. Park, J.-H. Jung, J. Kim, and B. Lee, "Color moiré pattern simulation and analysis in three-dimensional integral imaging for finding the moiré-reduced tilted angle of a lens array," Appl. Opt. **48**, 2178–2187 (2009).
16. V. V. Saveljev, J.-Y. Son, B. Javidi, S.-K. Kim, and D.-S. Kim, "Moiré minimization condition in three-dimensional image displays," J. Disp. Technol. **1**, 347–353 (2005).
17. V. V. Saveljev, J.-Y. Son, J.-H. Chun, and K.-D. Kwack, "About a Moiré-less condition for non-square grids," J. Disp. Technol. **4**, 332–339 (2008).
18. G. Lippmann, "La photographie integrale," C. R. Acad. Sci. **146**, 446–451 (1908).
19. F. Okano, H. Hoshino, J. Arai, and I. Yuyama, "Real-time pick-up method for a three-dimensional image based on integral photography," Appl. Opt. **36**, 1598–1603 (1997).
20. H. Hoshino, F. Okano, H. Isono, and I. Yuyama, "Analysis of resolution limitation of integral photography," J. Opt. Soc. Am. A **15**, 2059–2065 (1998).
21. P. S. Theocaris, "Radial gratings as moiré gauges," J. Phys. E **1**, 613–618 (1968).
22. M. Abolhassani and M. Mirzaei, "Unification of formulation of moiré fringe spacing in parametric equation and Fourier analysis methods," Appl. Opt. **46**, 7924–7926 (2007).
23. K. Patorski and S. Yokozeki, "Moiré profile prediction by using Fourier series formalism," Jpn. J. Appl. Phys. **15**, 443–456 (1976).
24. S. Yokozeki and K. Patorski, "Moiré fringe profile prediction method and its application to fringe sharpening," Appl. Opt. **17**, 2541–2547 (1978).
25. R. L. Zhao, W. X. Zhao, Q. H. Wang, D. H. Li, A. H. Wang, and Y. X. Xin, "Research on stereo viewing zone in autostereoscopic display based on parallax barrier," Acta Photon. Sin. **37**, 960–963 (2008) (in Chinese).